Poly(lactic acid)/Organoclay Nanocomposites: Thermal, Rheological Properties and Foam Processing

YINGWEI DI,[1] SALVATORE IANNACE,[1] ERNESTO DI MAIO,[2] LUIGI NICOLAIS[1,2]

[1]Institute of Composite and Biomedical Materials (IMCB-CNR), Piazzale Tecchio 80, 80125, Napoli, Italy

[2]Department of Materials and Production Engineering, University of Napoli "Frederico II," Piazzale Tecchio 80, 80125, Napoli, Italy

Received 18 May 2004; revised 2 November 2004; accepted 27 November 2004
DOI: 10.1002/polb.20366
Published online in Wiley InterScience (www.interscience.wiley.com).

ABSTRACT: In this study, polymer nanocomposites based on poly(lactic acid) (PLA) and organically modified layered silicates (organoclay) were prepared by melt mixing in an internal mixer. The exfoliation of organoclay could be attributed to the interaction between the organoclay and PLA molecules and shearing force during mixing. The exfoliated organoclay layers acted as nucleating agents at low content and as the organoclay content increased they became physical hindrance to the chain mobility of PLA. The thermal dynamic mechanical moduli of nanocomposites were also improved by the exfoliation of organoclay; however, the improvement was reduced at high organoclay content. The dynamic rheological studies show that the nanocomposites have higher viscosity and more pronounced elastic properties than pure PLA. Both storage and loss moduli increased with silicate loading at all frequencies and showed nonterminal behavior at low frequencies. The nanocomposites and PLA were then foamed by using the mixture of CO_2 and N_2 as blowing agent in a batch foaming process. Compared with PLA foam, the nanocomposite foams exhibited reduced cell size and increased cell density at very low organoclay content. With the increase of organoclay content, the cell size was decreased and both cell density and foam density were increased. © 2005 Wiley Periodicals, Inc. J Polym Sci Part B: Polym Phys 43: 689–698, 2005
Keywords: poly(lactic acid); organoclay; nanocomposites; melt mixing; exfoliation; thermal properties; rheological properties; foam processing

INTRODUCTION

Recently, much attention has been given to the study of polymer nanocomposites based on thermoplastic and organically modified layered silicates (organoclay). Within such materials, the layered organoclay particles are exfoliated and uniformly dispersed into the polymer matrix. With at least one dimension in nanoscale, these exfoliated platelets impart remarkably improved physical properties to the polymer nanocomposites as compared with the neat polymer matrix, as exemplified by high modulus, excellent gas barrier performance, as well as high heat deflection resistance.[1–3] These features of dispersed organoclay platelets mainly originate from their high affinity to the matrices that has been so far mostly obtained via modifying clay directly with a suitable alkylammonium salt. Interaction between polymer matrix and organoclay not only favors the exfoliation of organoclay stacks into

Correspondence to: Y. Di (E-mail: di@unina.it) or S. Iannace (E-mail: iannace@unina.it)

Journal of Polymer Science: Part B: Polymer Physics, Vol. 43, 689–698 (2005)
© 2005 Wiley Periodicals, Inc.

separated platelets but also property enhancements in nanocomposites.[4] Therefore, selection of a pair of polymer matrix and organoclay that has effective attraction to each other has become an essential criterion for making polymer nanocomposites. It has been shown that polymer nanocomposites with strong interaction between polymer matrix and organoclay also exhibited enhancement in melt viscosity and elasticity by forming a rubber-like interconnected structure without significant sacrifice on impact properties.[5–8] So making polymer nanocomposites containing a low amount of organoclay has become an effective way to modify the processing behavior of polymer matrix.

Poly(lactic acid) (PLA) is a biocompatible, environmentally friendly, biodegradable thermoplastic polymer that could be easily synthesized from renewable raw materials. The physical and mechanical properties of PLA rival those of many conventional petrochemical plastics, yet PLA degrades via simple mechanisms to lactic acid and low-molecular-weight oligomers, all of which are metabolized by both soil and marine organisms. Although traditionally used for biomedical applications, PLA is rapidly gaining recognition as biodegradable thermoplastics for general use applications, especially single-use packaging and consumer goods.[9] However, PLA has to have a high molecular weight in order to have acceptable mechanical properties, high melt viscosity, and melt strength/"elasticity" during processing in many applications such as flow molding and foam processing. Condensation polymerization is the least expensive route to produce commercial PLA, but it is difficult to obtain high molecular weights.

Herein, we report our effort to improve melt viscosity and elasticity of PLA by mixing it with organoclays to produce PLA nanocomposites with the expectation that the nanocomposites based on PLA will enlarge its application fields by the improvement of physical and mechanical properties. The influence of interaction between PLA and organoclay on the exfoliation of organoclays was compared by using two kinds of organoclays. The evidence resulting from the interaction between PLA and organoclay was investigated by exploring the thermal and rheological characterizations on PLA nanocomposites. These nanocomposites were then foamed in a batch process and their foaming behavior was compared with that of neat PLA. The nanocomposites based on PLA have been reported before by several research groups.[10–12] However, the unique behavior resulting from the interaction between nanoscale fillers and PLA matrix and physical foam processing of PLA nanocomposites are not well studied or yet reported.

EXPERIMENTAL

Materials

PLA, under the commercial name of Nature Works® 3000D from Cargill-Dow, UK, was used in this study as polymer matrix. The two types of organoclay, under the commercial names of Cloisite 30B and 93A (hereafter referred to as 30B and 93A, respectively) from Southern Clay Products Inc. (Gonzalez, TX), were used in the preparation of nanocomposites for the purpose of comparison. According to the product information from the producer, these two organoclays consisting of a same 2:1 montmorillonite (MMT) are organics-treated differently. 30B contains a quaternary ammonium ion containing methyl tallow bis-2-hydroxyethyl (MT2EtOT) and 93A contains methyl dehydrogenated tallow ammonium (M2HT) as the organic modifier.

Preparation of Samples

A Haake Rheomix® 600 internal mixer with two roller rotors was used for the preparation of the PLA/organoclay hybrids with different compositions. This mixer is attached to a measuring drive unit Haake Rheocord® 9000. The processing temperature was set at 170 °C. The rotor rotating speed and mixing time were fixed at 100 rpm and 10 min. The components were first dried in vacuum and then dry blended at predetermined compositions and subsequently melt mixed in the mixer under the protection of nitrogen atmosphere. After mixing, the samples were dumped out and compressed into about 2-mm-thick plates by a calender for further characterization.

Characterization

The wide-angle X-ray diffraction (WAXD) work was performed at ambient temperature by using a Philips X-ray generator and a Philips diffractometer, type PW1710, to evaluate the dispersibility of the organoclay layers in the PLA matrix. The X-ray beam was nickel-filtered Cu Kα radiation of wavelength 1.54 Å operated at the generator voltage of 40 kV and current of 20 mA. The

diffraction intensity data were collected automatically at a scanning rate of 0.6 °/min with 0.01 °/s steps. The organoclays were studied as powders and the hybrids were in flat films. The basal spacing of the organoclay was estimated from the (001) peak in the WAXD pattern using the Bragg's law, $d = \lambda/2\sin\theta_{max}$.

Differential scanning calorimetry (DSC) analysis was performed on a DSC2910 (TA Instruments, New Castle, DE). The instrument was calibrated with indium standard and nitrogen atmosphere was used throughout. The sample was weighed in the aluminum DSC pan and placed in the DSC cell. It was first heated from room temperature to 200 °C at 10 °C/min and kept at 200 °C for 3 min to eliminate the previous heat history and subsequently cooled to 20 °C at 10 °C/min. The sample was then heated again to 200 °C at 10 °C/min. This second heating process was regarded as melting scan for the analysis. The crystallization and melting temperatures were determined as the temperatures at the maximum values of crystallization and melting peaks.

The dynamic mechanical analysis (DMA) was performed using a model DMA983 dynamic mechanical analyser (TA Instruments). The testing was performed in three-point bending mode at a vibration frequency of 1 Hz in the temperature range from 0 to 160 °C at a heating rate of 10 °C/min in N_2 atmosphere.

Dynamic rheological measurements were performed using an advanced rheometric expansion system (ARES) rheometer from Rheometric Inc. (Piscataway, NJ). The measurements were performed in an oscillatory shear mode using parallel plate geometry 25 mm in diameter at 170 °C under nitrogen atmosphere. Frequency sweeps between 0.01 and 100 rad/s were performed at low strains (0.1–10%) which have been shown to be within the linear viscoelastic range of the measured samples. The time sweep tests at test temperature had also been performed before the frequency sweep to ensure no significant thermal degradation occurred within the experimental time. Specimens were placed between the preheated plates at experimental temperature and were allowed to equilibrate before each frequency sweep run. The obtained values were calculated according to the true gap between the plates.

Foaming Processing and Cellular Structure Analysis

The basic principle of a physical foaming process on polymer is to dissolve a blowing agent (typically a gas) into a polymer matrix and then reduce the solubility of the blowing agent by thermodynamic instabilities, usually a temperature increase or a pressure decrease, to induce the nucleation. After nucleation, the bubble growth starts, which is mainly controlled by the temperature. The foam cells are finally vitrified when the temperature is reduced, usually below the glass-transition temperature of the polymer matrix.[13] In this study, the physical foaming (batch process) was conducted in a high-pressure stainless-steel autoclave made by HiP (Erie, PA). PLA and PLA nanocomposites, in the form of pellets or a compression-molded plaque, were dried, weighed, and placed on the sample holder inside the autoclave. The flowing agent used in this study was a compressed mix of gases CO_2 and N_2 (20:80) (Aligal® 12 by Air Liquide, Italy). Before a typical experiment, the autoclave was flushed with flowing agent for a few seconds and then pressurized with flowing agent to the desired saturation pressure and heated to the foaming temperature (~110 °C). The pressure and temperature signals were monitored using a pressure transducer and a thermocouple, respectively, mounted inside the autoclave and indicated on a digital display outside the autoclave. The solubilization time, about 4 h, was maintained to ensure equilibrium absorption of blowing agent by the samples and then the pressure was rapidly reduced (about 2 s) to atmosphere pressure. After the pressure releasing, the foams were cooled naturally to room temperature and then carefully removed from the autoclave and kept in a desiccator at room temperature. The cell structure of the resulted foams was analyzed using a LEICA scanning electron microscope (SEM) model S440. The SEM samples were prepared by cryogenically cutting the obtained foam samples and gold sputtering the fractured cross-sections. The average cell size, d, in micron was obtained by measuring the maximum diameter of each cell perpendicular to the skin from SEM micrographs. To determine the cell-size distribution, the size of at least 50 cells in an SEM micrograph was measured. The bulk densities of both prefoamed, ρ_p, and postfoamed, ρ_f, samples in g/cm^3 were estimated by using the method of buoyancy. The cell densities, Nc, in cells/cm^3 are defined in eq 1[14]:

$$Nc \approx 10[1 - (\rho_f / \rho_p)] / d^3 \quad (1)$$

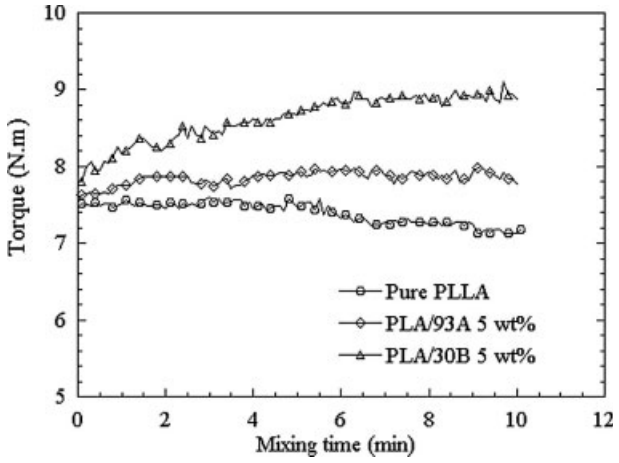

Figure 1. Mixing torque variation with the mixing time for pure PLA, PLA/30B, and PLA/93A hybrids.

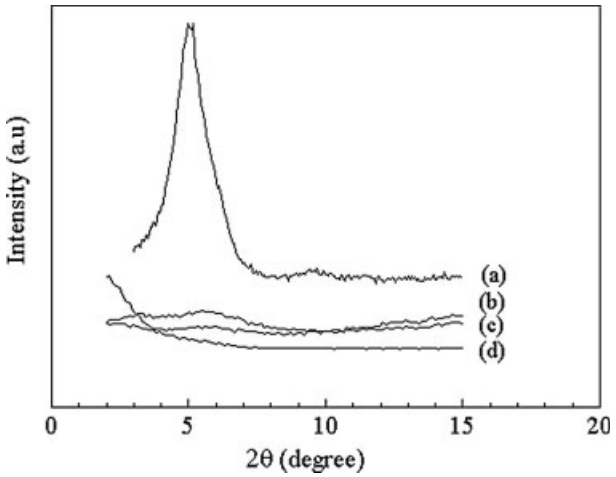

Figure 2. WAXD patterns: (a) 30B; (b) PLA/2 wt % 30B; (c) PLA/5 wt % 30B; (d) PLA/10 wt % 30B.

RESULTS AND DISCUSSION

Hybrid Structure from Melt Mixing

During the melt-mixing process, the torque variation with mixing time is the first indication of the structure formation of hybrids. In Figure 1, the corresponding diagram for PLA/30B and PLA/93A hybrids with the same organoclay composition is presented as an example, in which the torque variation with mixing time for pure PLA resin is also shown for the purpose of comparison. It can be seen that the mixing torques of hybrids are always higher than those of neat PLA because of the existence of rigid fillers of organoclay. The mixing torque of PLA/30B hybrid is steadily higher than that of PLA/93A, reflecting high shear stress caused by mixing PLA and 30B.

The structure of the resulting hybrids was further determined by WAXD analysis. In Figure 2, the WAXD patterns of the organoclay 30B and some PLA/30B hybrids with different 30B compositions were compared. The primary silicate reflection at $2\theta = 5.02°$ of 30B powder corresponds to a layer spacing of 1.76 nm which is higher than 1.1 nm of original MMT because of the insert of organic modifier. For the PLA/30B hybrids with 2, 5, and 10 wt % of 30B, there are no noticeable WAXD peaks of 30B observed at low-angle range, confirming that the disordered, exfoliated structures of silicate layers of 30B in PLA matrix were obtained after melt mixing. In contrast to PLA/30B hybrids, the diffraction patterns of 93A and PLA/93A hybrid in Figure 3 showed that after melt mixing with PLA the main characteristic diffraction peak of 93A shifted to lower angle at $2\theta = 2.9°$ ($d \approx 3.04$ nm) from $2\theta = 3.8°$ ($d \approx 2.32$ nm), whereas its intensity was almost unchanged. These observations indicate that the layer spacing of 93A was slightly increased but its ordered structure was not disrupted after melt mixing. A small weak peak that appeared around $2\theta = 5.9°$ [Fig. 3(b)] is due to the second registry (d_{002}) of MMT clay.[15,16] From the WAXD analysis, we can conclude that 93A was not exfoliated or significantly intercalated after mixing with PLA so PLA/93A hybrids yielded microcomposites. Such structure differences were similar to those we observed in polycaprolactone (PCL)/30B and PCL/93A hybrids,[8] which could be attributed to the interaction of hydrogen-bonding between the

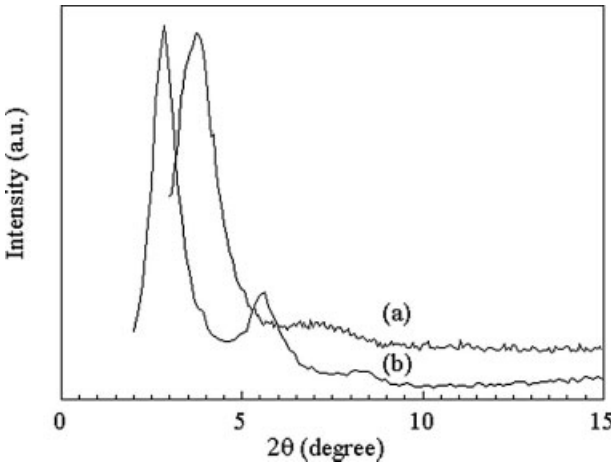

Figure 3. WAXD patterns: (a) 93A; (b) PLA/5 wt % 93A.

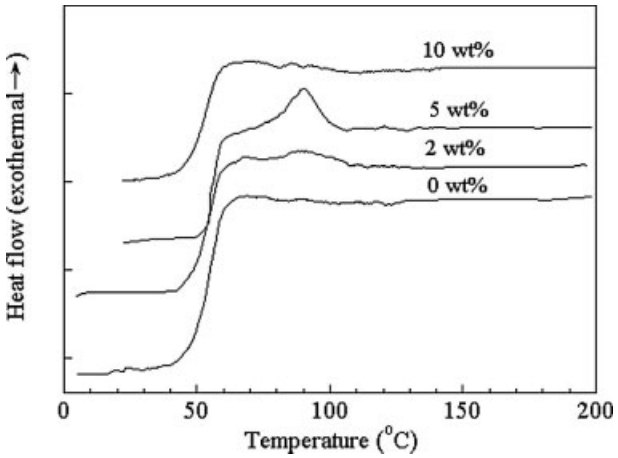

Figure 4. DSC cooling thermograms at −10 °C/min for PLA and PLA/30B nanocomposites with different weight fractions of 30B.

carbonyl group in the main chain of PLA molecules and the hydroxyl group in the organic modifier of 30B is much higher than that between no polar organic modifier in 93A and PLA matrix. The strong interaction between PLA and 30B also caused a higher mixing torque than that of the PLA/93A hybrid (Fig. 1) which leads to more significant delamination of 30B for PLA/30B nanocomposite formation. We thereafter selected 30B as the organoclay for preparing PLA nanocomposites and the following content is focused only on PLA/30B nanocomposites.

Crystallization and Melting Behavior

It is well known that PLA crystallizes slowly compared with other polyesters such as PCL and polyethylene terephthalate because of the rigid segments in its main chain.[17] In Figure 4 we can see that, at the cooling rate of 10 °C/min, the pure PLA does not crystallize, therefore no crystallization peak is visible in its cooling thermogram. This result implies that the pure PLA samples cooled from the isotropic melt at a cooling rate more than 10 °C/min remain amorphous. However, for 2 and 5 wt % 30B nanocomposites, crystallization peaks of PLA were observed with the peak temperatures around 90 °C. These results clearly show that small amounts of 30B exfoliated in PLA matrix result in an obvious increase of the crystallization rate as compared with the pure PLA. This behavior can be explained by the assumption that the exfoliated silicate layers act as efficient nucleating agents, which enhance the crystallization rate of the matrix molecules, and this effect will be increased with the increasing of the organoclay contents because of the increased amount of nucleating agents.[18] However, at 10 wt % of 30B, the crystallization peak of PLA does not appear. A similar behavior was also shown in the melting process for PLA and PLA/30B nanocomposites. In Figure 5 we see that the nanocomposites showed lower crystallization temperatures than that of pure PLA because of the nucleating effect of well-dispersed organoclay 30B layers. Among them, the 5 wt % 30B nanocomposite shows the lowest crystallization temperature, even lower than that of the 10 wt % 30B nanocomposite. Such behavior could be regarded as unique for polymer nanocomposites in which there exists strong interaction between polymer matrix and nanoscale fillers. Because of the strong interaction between organic surfactant covered on the surface of platelets of 30B and the functional groups on the main chain of PLA molecules, polymer chains attached to the platelets are partially immobilized and hindered from taking part in the flow process and their crystallization process. The higher the content of organoclay added, the more interacting sites would be resulted in for the reduction of the mobility of the PLA molecules. Accordingly, other than nucleation agents, the exfoliated organoclay layers can also become retardant of crystallization acting as physical hindrance if there exists the strong interaction between polymer matrix and organoclay. The former effect is pronounced at low organoclay content and as the organoclay content is increased the latter effect will become dominant.[8]

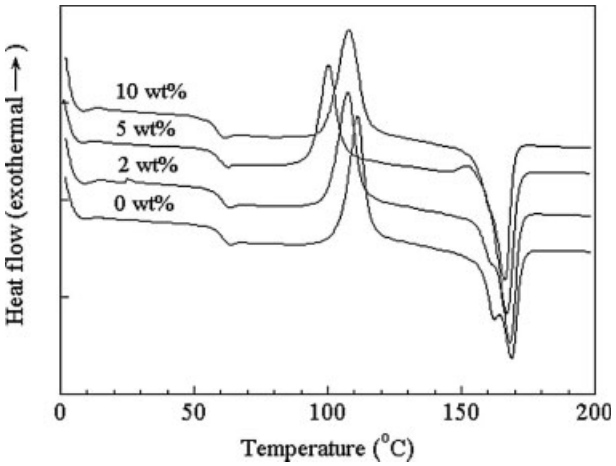

Figure 5. DSC melting thermograms of PLA and PLA/30B nanocomposites with different weight fractions of 30B.

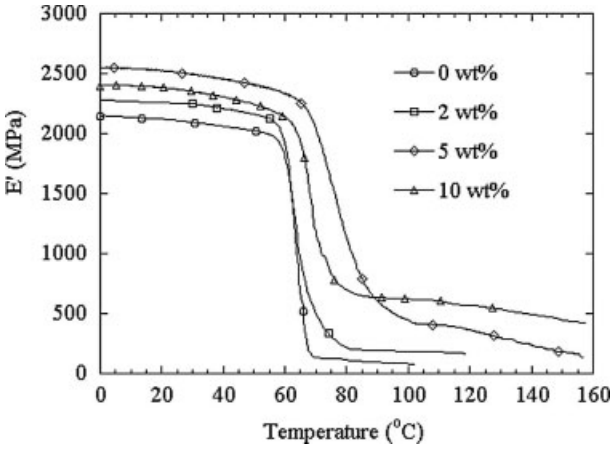

Figure 6. Temperature dependence of E' for PLA and PLA/30B nanocomposites with different weight fractions of 30B.

In Figure 5 we can also see that the melting endothermic graph of PLA shows two peaks but the PLA/30B nanocomposites all show one melting peak corresponding to the primary melting peak of PLA. This implies that addition of 30B not only affects the crystallization rate of PLA but also its crystal forms. The melting peak temperatures of PLA in PLA/30B nanocomposites did not change significantly with the content of 30B.

DMA

DMA was used to investigate the thermomechanical properties of PLA and its nanocomposites. The temperature dependence of the dynamic storage modulus, E', corresponding to the elastic response to the deformation, for pure PLA and PLA/30B nanocomposites, is depicted in Figure 6. In the investigated temperature range, nanocomposites exhibit higher storage modulus than that of the pure PLA, indicating that addition of organoclay into PLA matrix results in a remarkable increase of elastic properties for PLA nanocomposites. At higher temperatures, more than 80 °C, the E' curves for the nanocomposites display a more improved plateau than pure PLA, which means an increase of thermal-mechanical stability for the nanocomposites at high temperatures.

In Figure 6, one interesting phenomenon noted is that the nanocomposite with 5 wt % 30B shows the highest E' value, even higher than that with 10 wt % 30B, at temperatures less than 90 °C before the nanocomposites become soft. It has been well known that the mechanical properties of a filled system depend on two principal factors: crystallinity of the polymer matrix and the extent of filler reinforcement. The degree of crystallinity must be considered in the analysis of this phenomenon. The WAXD diffractograms of pure PLA and its nanocomposites were compared in Figure 7 where we can see that the crystallinity of 5 wt % 30B nanocomposites is the highest among the samples. Therefore, the enhanced crystallinity in the PLA/30B (5 wt %) nanocomposite contributes more to the improvement of mechanical properties than the increased content of 30B in nanocomposites of 10 wt % 30B. At higher temperatures (>90 °C), when materials become soft, the reinforcement effect of the exfoliated 30B particles becomes prominent because of the restricted movement of the polymer chains and hence the modulus is increased with the organoclay content.

This improved strength has also been observed for other polymer/clay nanocomposites, which depends on the degree of intercalation of polymer chains and/or exfoliation of clay and the improvement usually increases with the increasing of clay content.[19,20] In the case of PLA nanocomposites in this study, such unique behavior that the crystallinity contributes more to the improvement of mechanical properties than the content of 30B does could also be attributed to both the strong interaction between the organoclay 30B and PLA molecules and good dispersion of 30B platelets in the PLA matrix.

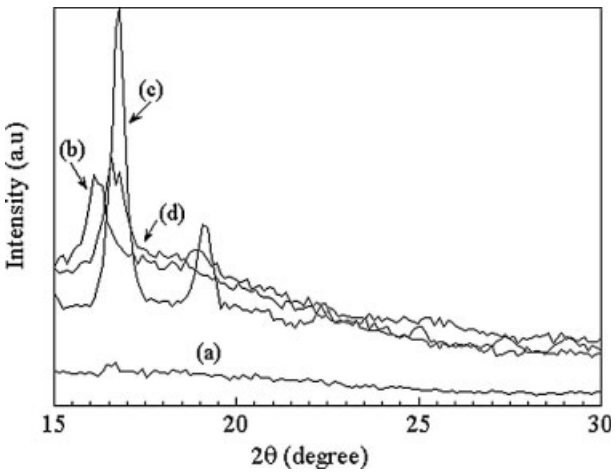

Figure 7. WAXD patterns for PLA and PLA nanocomposites with different weight fraction of 30B: (a) PLA; (b) PLA/2 wt % 30B; (c) PLA/5 wt % 30B; (d) PLA/10 wt % 30B.

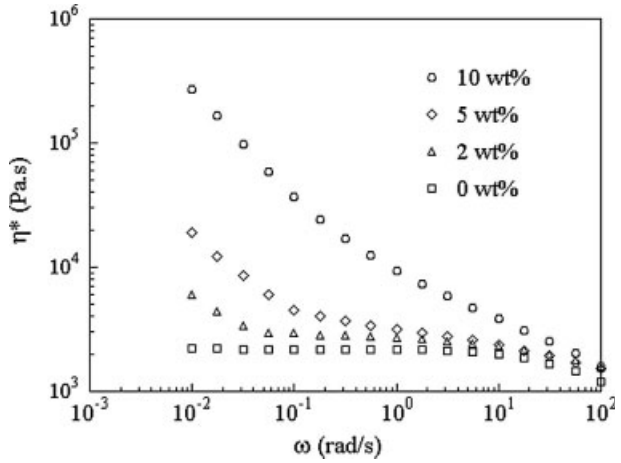

Figure 8. Complex viscosity curves of PLA and PLA/30B nanocomposites with different weight fractions of 30B at 170 °C.

Rheological Properties

The dynamic oscillatory shear measurements were performed on PLA and its nanocomposites to investigate the response of the nanostructure to the dynamic shearing. The complex viscosities, η^*, of the pure PLA and PLA/30B nanocomposites as a function of frequency, ω, are shown in Figure 8. The η^* of the PLA melt shows only a small frequency dependence, revealing a Newtonian plateau at low frequency. The η^* of the nanocomposites is overall higher than that of the neat PLA within the frequency range studied and η^* increases with the organoclay content, showing that the effect of the exfoliated organoclay layers on the complex viscosity is very pronounced. The nanocomposites' viscosity curves have a steep slope and there is no Newtonian plateau at low frequencies. In the conventional filled polymer systems, the disappearance of the Newtonian plateau at low frequencies usually takes place at much higher filler loadings than those in the PLA/30B nanocomposites, indicating the significant effect of nanoscale dispersion of the organoclay layers on the melt viscosity.[21] This is in accordance with experimental observations for other PLA/clay nanocomposites that the enhanced melt viscosity could be attributed to the flow restrictions of PLA chains caused by the strong interaction between 30B and PLA molecules.[12]

The storage modulus, G', and loss modulus, G'', for PLA nanocomposites were also increased as compared with pure PLA. In Figure 9 we can see that G' and G'' of the nanocomposites all show the plateau and increase with 30B content at low frequency range and then they become close, respectively, at high frequency range. It is well known that interconnected structures with anisometric fillers result in an apparent yield stress which is visible in dynamic measurement by a plateau of G' or G'' versus frequency at low frequencies.[8,22] This effect is more pronounced in G' than in G''. In Figure 9 we see that starting at about 2 wt % 30B, G' seems to reach a plateau at low frequencies. Therefore, an interconnected structure is assumed to be formed in PLA nanocomposites originated from the strong interaction between PLA molecules and 30B. As 30B content increases, the connectivity is more pronounced, as seen in the enhanced melt elasticity in Figure 9.

Foam Processing and Cellular Structure

The improved elastic and viscous properties for PLA nanocomposites encouraged us to perform

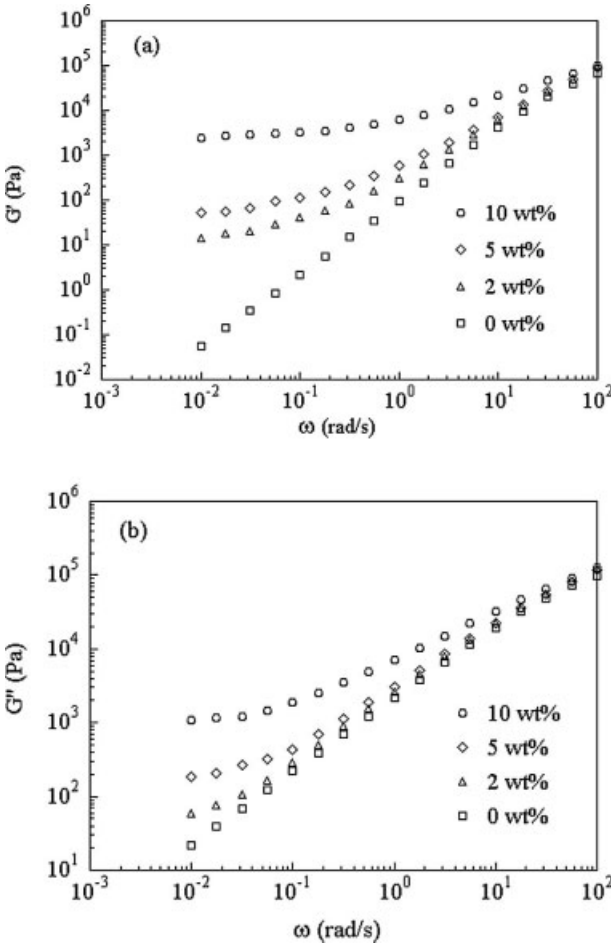

Figure 9. G' (a) and G'' (b) versus frequency for PLA and PLA nanocomposites with different weight fractions of 30B at 170 °C.

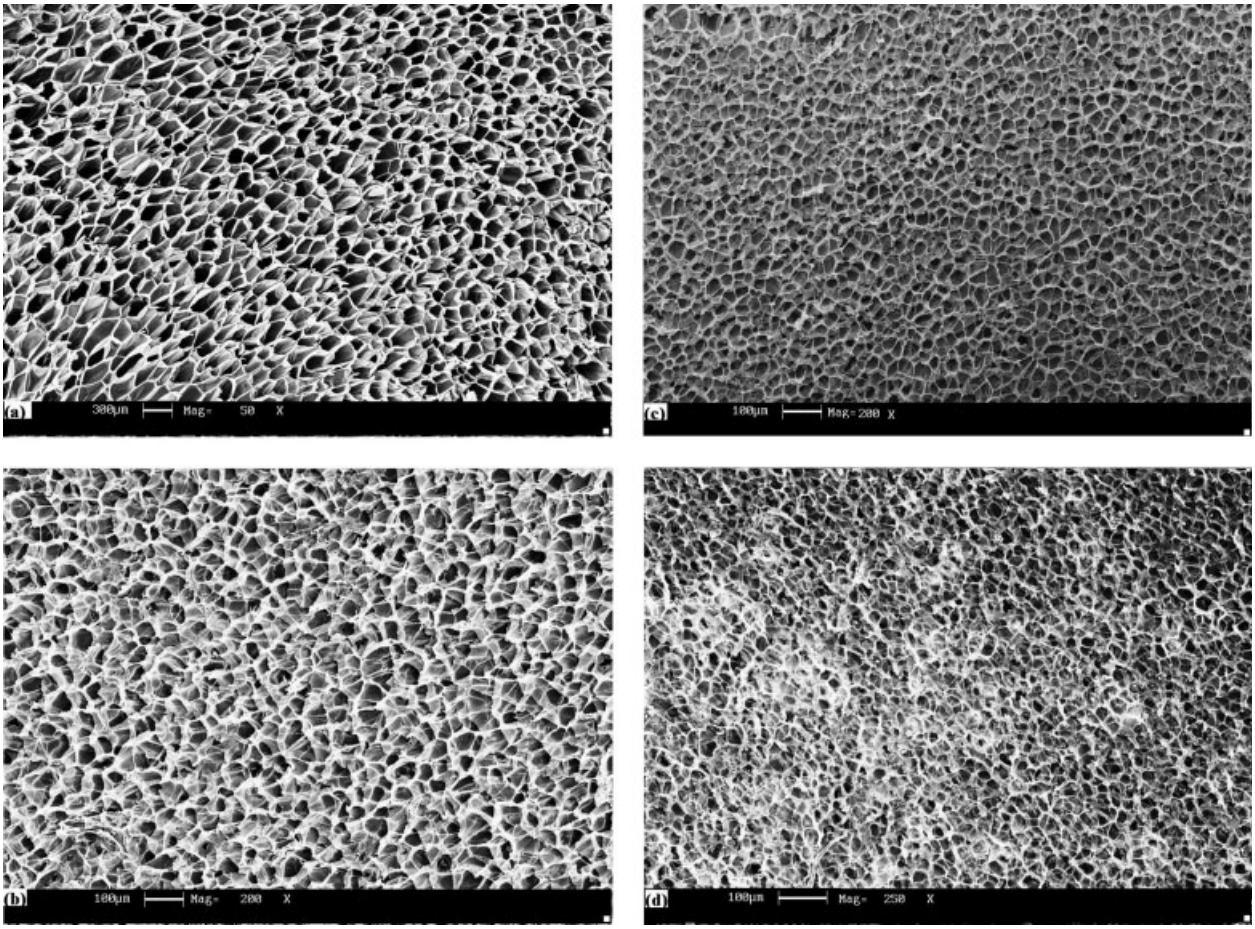

Figure 10. SEM micrographs for foams of PLA and PLA nanocomposites with different weight fraction of 30B: (a) PLA, original magnification 50×; (b) PLA/1 wt % 30B, original magnification 200×; (c) PLA/2 wt % 30B, original magnification 200×; (d) PLA/5 wt % 30B, original magnification 250×.

foam processing on them. In Figure 10, the SEM images of foamed PLA and PLA nanocomposites are shown. We can see that, under the same foaming condition, finely dispersed cells were formed in foams of PLA and PLA nanocomposites. The foams of PLA nanocomposites exhibited a nicely interconnected, closed-cell structure with pentagonal and hexagonal faces, which express the most energetically stable state of polygon cells. The foam structure may thus be best described by a packing of pentagonal dodecahedra or tetrakaidecahedra.[23,24] Such foam structure is different from that blown by sole CO_2 [25] because of higher gas phase volume (>0.74) by using a mixture of CO_2 and N_2 as blowing agent in this study.[13]

We note that the cell size of pure PLA foam is very large ($d \approx 230$ μm) and it decreases greatly even with a small amount of 30B (1 wt %), as shown in Figure 11, and then levels off at higher 30B concentration. This behavior is attributable to the intrinsically high viscosity of the nanocomposites subjected to foam processing, as seen in Figure 8, which restricts the expansion of cells. Although the test temperature is not the actual foaming temperature, 110 °C, these results can provide some general trend. Under the organoclay effect, the high moduli might also restrict the cell growth; as we have seen in Figure 6, the elastic moduli at 110 °C are 176 MPa for PLA2, 400 MPa for PLA5, and 600 MPa for PLA10. The 10 wt % 30B nanocomposite was poorly foamed at the same foaming condition because of much higher viscosity and elastic modulus than others.

The bulk foam densities were measured and found to be significantly reduced compared with the prefoamed samples. The cell densities were then calculated based on these foam densities according to eq 1 and shown in Figure 11, where

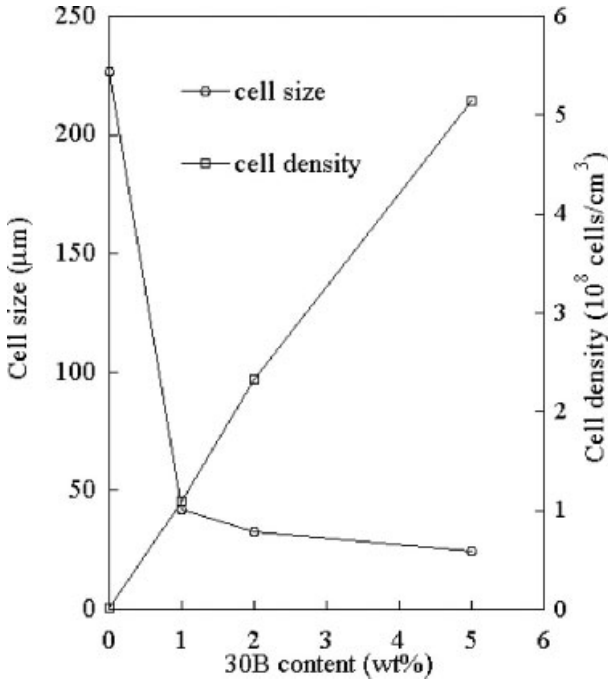

Figure 11. The cell size and cell density of PLA nanocomposite foams with different weight fractions of 30B.

we see that the cell density is relatively low for pure PLA foam and it increases nearly linearly with the organoclay content (from 0.0081 $\times$ 10^8 cell/cm^3 for pure PLA to 5.1 $\times$ 10^8 cell/cm^3 for PLA/5 wt % 30B). It has been well shown in the above sections that finely dispersed organoclay layers and more disposed surface area induced heterogeneous nucleation in the PLA matrix. According to the classical nucleation theory,[26–28] these heterogeneous nucleation agents contribute to cell nucleation during the foaming process by reducing the nucleation energy resulting from the difference of interfacial tension at the polymer-additive-gas interface. Because of the large surface area caused by organoclay exfoliation, such surface tension differences may well exist in PLA nanocomposites with different 30B contents. Therefore, the more organoclay exfoliated in the PLA matrix, the more cell nucleation sites are created and thus the cell density increases with organoclay content in foams of PLA/30B nanocomposites.

We calculated and compared the distribution function of cell size from these SEM images. The samples obeyed the Gaussian distribution and the width of the distribution peaks, which indicates the dispersion state for cell size, became narrower with increasing 30B content. This behavior is also attributable to the heterogenous organoclay layers that act as nucleation sites and their uniform dispersion in the PLA matrix, which lead to the high homogeneity of cell size.

CONCLUSIONS

The exfoliation of one organoclay in PLA matrix has been achieved by melt mixing in an internal mixer. The strong interaction between the organoclay and polymer matrix and shearing force during mixing are confirmed as two essential factors for PLA/30B nanocomposite fabrication.

Because of the strong interaction between PLA and 30B, the PLA molecules at the surface of the nanoscale 30B layers are partially immobilized. Because of the high surface area of nanoscale 30B layers, the effects from reduced molecular mobility become significant, leading to unique properties for the PLA nanocomposites. The exfoliated organoclay platelets act as nucleating agents at low content by increasing the crystallization rate of PLA. However, at high organoclay content, they become the crystallization retardant acting as physical hindrance to restrict the molecular chain mobility of PLA because of the increased interaction sites. The existence of nanometer-scale layers also improved thermomechanical dynamic storage modulus, E', and induced a wider plateau of E' over PLA glass-transition temperature for the PLA nanocomposites. However, further increase (>5 wt %) of organoclay content does not lead to an increase of E' because of the reduced crystallinity in the PLA nanocomposite. Therefore, there is an optimal amount of organoclay for nanocomposites to achieve the greatest improvements in their properties.

The melt viscosity and dynamic shear modulus of nanocomposites are also enhanced significantly by the exfoliation of organoclay. The dynamic shear storage modulus, G', and loss modulus, G'', exhibited less frequency dependence than pure PLA at a low frequency range. These results have been attributed to the strong interaction between PLA and exfoliated organoclay layers which lowers the molecular mobility of PLA and forms an interconnected structure within the PLA matrix.

The improvements of viscous and elastic properties for PLA/30B nanocomposites promise them a successful application in foam processing, allowing us to produce PLA foams with much smaller cell size and higher cell density than those of pure PLA even at low 30B content. It is reasonable to

expect that by controlling the organoclay content and processing conditions, the PLA foams with different cellular structures could be obtained for various purposes of application.

REFERENCES AND NOTES

1. Vaia, R.; Krishnamoorti, R. In Polymer Nanocomposite; Krishnamoorti, R.; Vaia, R., Eds.; American Chemical Society: Washington, DC, 2001; Chapter 1, pp 1–7.
2. Giannelis, E. P. Adv Mater 1996, 8, 29–35.
3. Alexandre, M.; Dubois, P. Mater Sci Eng 2000, 28, 1–63.
4. Fornes, T. D.; Yoon, P. J.; Hunter, D. L.; Keskkula, H.; Paul, D. R. Polymer 2002, 43, 5915–5933.
5. Lim, Y. T.; Park, O. Macromol Rapid Commun 2000, 21, 231–235.
6. Krishnamoorti, R.; Giannelis, E. P. Macromolecules 1997, 30, 4097–4102.
7. Fornes, T. D.; Yoon, P. J.; Hunter, D. L.; Keskkula, H.; Paul D. R. Polymer 2002, 43, 5915–5933.
8. Di, Y.; Iannace, S.; Di Maio E.; Nicolais, L. J Polym Sci Part B: Polym Phys 2003, 41, 670–678.
9. Drumright, R. E.; Gruber, P. R.; Henton, D. E. Adv Mater 2000, 12, 1841–1846.
10. Paul, M.; Alexandre, M.; Degée, P.; Henrist, C.; Rulmont, A.; Dubois, P. Polymer 2003, 44, 443–450.
11. Chang, J. H.; An, Y.; Sur, G. S. J Polym Sci Part B: Polym Phys 2003, 41, 94–103.
12. Ray, S. S.; Okamoto, M. Prog Polym Sci 2003, 28, 1539–1641.
13. Klempner, D.; Frisch, K. C. Handbook of Polymeric Foams and Foam Technology; Hanser: Munich, 1991.
14. Nam, P. H.; Maiti, P.; Okamoto, M.; Kotaka, T. Polym Eng Sci 2002, 42, 1907–1918.
15. Ray, S. S.; Maiti, P.; Okamoto, M.; Yamada, K.; Ueda, K. Macromolecules 2002, 35, 3104–3110.
16. Pluta, M.; Galeski, A.; Alexandre, M.; Paul, M. A.; Dubois, P. J Appl Polym Sci 2002, 86, 1497–1506.
17. Miyata, T.; Masuko, T. Polymer 1998, 39, 5515–5521.
18. Zhang, G.; Yan, D. J Appl Polym Sci 2003, 88, 2181–2188.
19. Xu, M.; Choi, Y. S.; Kim, Y. K.; Wang, K. H.; Chung, I. J. Polymer 2003, 44, 6387–6395.
20. Nam, P. H.; Maiti, P.; Okamoto, M.; Kotaka, T.; Hasegawa, N.; Usuki, A. Polymer 2001, 42, 9633.
21. Hoffmann, B.; Dietrich, C.; Thomann, R.; Friedrich, C.; Rolf, M. Macromol Rapid Commun 2000, 21, 57–61.
22. Shenoy, A. V. Rheology of Filled Polymer Systems; Kluwer Academic: New Dehli, 1999.
23. Chan, R.; Nakamura, M. J Cell Plast 1969, 5, 112.
24. Renz, R.; Ehrenstein, G. W. Cell Polym 1982, 1, 5.
25. Fujimoto, Y.; Ray, S. S.; Okamoto, M.; Ogami, A.; Yamada, K.; Ueda, K. Macromol Rapid Commun 2003, 24, 457–461.
26. Colton, J. S.; Suh, N. P. Polym Eng Sci 1987, 27, 485–492.
27. Colton, J. S.; Suh, N. P. Polym Eng Sci 1987, 27, 493–499.
28. Colton, J. S.; Suh, N. P. Polym Eng Sci 1987, 27, 500–508.